Electronic structure of [100]-oriented free-standing InAs and InP nanowires with square and rectangular cross sections

M. P. Persson[1,2,*] and H. Q. Xu[1,†]
[1]*Division of Solid State Physics, Lund University, P.O. Box 118, S-221 00 Lund, Sweden*
[2]*Dipartimento di Ingegneria Elettronica, Università di Roma "Tor Vergata," Via del Politecnico 1, 00133 Roma, Italy*
(Received 26 November 2005; published 29 March 2006)

We report on a theoretical study of the electronic structure of free-standing InAs and InP nanowires grown along the [100] crystallographic direction, based on an atomistic tight-binding approach. The band structure and wave functions for nanowires with both square (nanowires) and rectangular (nanobelts) cross sections are calculated. A comparison is made between the calculations for InAs, InP, and GaAs nanowires and similar characteristics are found in the band structure and wave functions of the three material types of nanowires. It is found that the nanowires with both square and rectangular cross sections have simple, parabolic conduction bands. However, the characteristics of the valence bands in the nanowires are found to be cross-section aspect-ratio dependent. For the nanowires with a square cross section, the valence bands show rich and complex structures. In particular, the highest valence band of a square nanowire shows a double-maximum structure and has its energy maximum at $k \neq 0$, giving an indirect nanowire band gap. When the cross section of the nanowires changes from a square to a rectangular type, the top valence bands tend to develop into parabolic bands. For the nanowires with the same cross-section aspect ratio and material type, the valence band structures at different sizes are found to have similar characteristic structures, although the band energies sensitively depend on the nanowire lateral size. The wave functions of the band states of the InAs and InP nanowires at the Γ point have been calculated. It is found that for the square nanowires the valence band states show complex structures. For the rectangular nanowires with sufficiently large aspect ratios the wave functions of the topmost valence band states show the features predicted by a one-band effective-mass model, in agreement with the fact that these valence bands become good parabolic bands in these rectangular nanowires.

DOI: 10.1103/PhysRevB.73.125346 PACS number(s): 73.22.Dj, 73.21.Hb

I. INTRODUCTION

In recent years, nanometer-scale free-standing semiconductor wires have attracted great attention, due to their well-defined crystalline structure and unique electrical and optical properties.[1–17] Common methods for the growth of free-standing nanowires are the so-called vapor-liquid-solid[1,2] (VLS) and vapor-solid-solid[3] (VSS) growth methods, where metal particles act as catalysts for the nanowire growth. These growth methods have been applied to a wide variety of materials, such as III-V semiconductor compounds, Si, Ge, CdS, and ZnO. Typical dimensions of these nanowires are in the order of a few to 100 nm in diameter and several micrometers in length. For free-standing III–V nanowires, grown using the VLS or VSS mechanism, a common growth direction is the [111] crystallographic direction,[4] although recently results showing controlled growth along the $\langle 100 \rangle$ directions have been reported.[5] The growth techniques for this type of nanowire have been well developed during the last two decades and it is now possible to create high quality nanowires with controlled length and diameter.[6] It is also possible to dope the nanowire[7] and to create nanowire heterostructures.[8] Based on these technical achievements, devices such as nanowire diodes,[4,9] light-emitting diodes (LEDs),[4,7,9] resonant tunneling diodes,[10] superlattices,[11,12] and electrically driven lasers[17] have been realized and demonstrated.

For further development and optimization of these devices it is important to have theoretical models which provide information about the electronic structure as well as the optical and mechanical properties of the nanowires. The structures considered in such models often have large unit cells, each containing a large number of atoms, which makes first principles calculations impractical. For sufficiently large systems the $\mathbf{k}\cdot\mathbf{p}$ approach generally generates accurate solutions for the states around the Γ point with near band-gap energies. However, as a nonatomistic model the $\mathbf{k}\cdot\mathbf{p}$ method will sometimes overestimate the symmetry of the system and the effects of quantum confinements. The tight-binding approach has, as an atomistic approach, the advantages of accurately describing the band structure through the whole Brillouin zone and of correctly taking into account the crystal symmetry of the system. Even though the size of the tight-binding Hamiltonian scales linearly with the number of atoms, it is now possible to handle a nanowire with a unit cell containing $\sim 10^6$ atoms using the fact that the Hamiltonian is highly sparse.

Theoretical studies based on $\mathbf{k}\cdot\mathbf{p}$ models have been carried out for cylindrical and/or embedded nanowires.[18–21] The majority of the work found in the literature concerns lithographically and epitaxially defined wires such as *V* groove, *T* shaped, and etched wires,[22–25] with the crystallographic orientation along the $\langle 011 \rangle$ directions. Regarding free-standing systems, calculations for nanowires grown along the [111] direction based on $\mathbf{k}\cdot\mathbf{p}$ theory,[20,26] tight-binding, and pseudopotential methods[27–31] have been reported. Along the $\langle 100 \rangle$ directions the studies have been carried out using $\mathbf{k}\cdot\mathbf{p}$ theory for nanowires with circular cross sections,[20] the pseudopo-

TABLE I. Properties of the InAs and InP bulk materials as produced by the tight-binding parameters used in this work. The values are taken from Ref. 35.

Material	E_g(eV)	Δ_{SO} (eV)	m_e^*	m_{lh}^* [001]	m_{lh}^* [110]	m_{hh}^* [001]	m_{hh}^* [110]	m_{SO}^*
InAs	0.368	0.381	0.024	−0.028	−0.027	−0.364	−0.657	−0.098
InP	1.345	0.105	0.078	−0.082	−0.076	−0.480	−0.886	−0.150

tential method for nanowires with very small sizes,[29,32] and the tight-binding method for GaAs nanowires and GaAs/AlGaAs nanowire superlattices.[33,34]

Previous theoretical studies of III-V semiconductor nanowires have been concentrated on GaAs material system. However, much of the current experimental work is being performed on other material systems, such as InAs and InP. To examine to what extent the electronic structure of nanowires made of different III-V materials could differ, we study the electronic structure of nanowires made from InAs with a small bulk band gap and low electron and light-hole effective masses and from InP with bulk band-gap and effective-mass values comparable to GaAs.

Our calculations for the electronic structure of the freestanding InAs and InP nanowires oriented along the [100] crystallographic direction are carried out based on an atomistic nearest-neighbor tight-binding model.[35] Here the sp^3s^* basis set proposed by Vogl *et al.*[36] is employed. The model, which has the advantage of using a small basis set of atomic orbitals, reproduces the band structure of both the conduction and the valence bands of bulk crystal with a good accuracy. The results of calculations for the band structure and state wave functions of the InAs and InP nanowires with both square and rectangular cross sections are presented. The band structure and wave functions of InP, InAs, and GaAs nanowires are compared and the differences and common features in the electronic structure of these nanowire systems are discussed.

II. THEORY AND MODEL

A. Method

In this work an sp^3s^* tight-binding nearest-neighbor parameter set with the inclusion of spin-orbit interaction[35] is employed in the calculations of the electronic structure for the freestanding InAs and InP nanowires. The tight-binding parameter set was obtained by fitting to both the band energies and the effective masses of the bulk materials. The bulk InAs and InP material properties produced by this tight-binding parameter set are collected in Table I. The tight-binding parameters used in this work and additional properties of the bulk materials can be found in Ref. 35.

The nanowires are assumed to be infinitely long. Consequently the Hamiltonian matrix for each nanowire is expressed in a basis of Bloch sums,

$$|\alpha,\mathbf{k}\rangle = \frac{1}{\sqrt{N}}\sum_{\mathbf{R}} e^{i\mathbf{k}\cdot\mathbf{R}_\alpha}|\mathbf{R}_\alpha,\alpha\rangle, \tag{1}$$

with $\mathbf{R}_\alpha=\mathbf{R}+\mathbf{r}_\alpha$, where $\mathbf{R}$ is a lattice vector, $\mathbf{r}_\alpha$ is an atomic displacement vector in a unit cell, N is the number of lattice sites, and $|\mathbf{R}_\alpha,\alpha\rangle$ stands for an atomic orbital α at $\mathbf{R}+\mathbf{r}_\alpha$. In this basis the tight-binding Hamiltonian in $\mathbf{k}$ space becomes

$$\mathbf{H}_{\alpha,\beta}(\mathbf{k}) = \sum_{\mathbf{R}} e^{-i\mathbf{k}\cdot(\mathbf{R}'_\alpha-\mathbf{R}_\beta)}\langle\mathbf{R}'_\alpha,\alpha|\boldsymbol{H}|\mathbf{R}_\beta,\beta\rangle, \tag{2}$$

and the eigenfunctions can be expressed as

$$|n,\mathbf{k}\rangle = \sum_{\alpha} c_{n\alpha}|\alpha,\mathbf{k}\rangle, \tag{3}$$

where the sum of α needs to be run through all the atomic orbitals included in the unit cell.

The nonzero, nonequivalent interaction parameters between atomic orbitals with the same spin are

$$E_{j,s} = \langle j,s|\mathbf{H}|j,s\rangle, \quad E_{j,s^*} = \langle j,s^*|\mathbf{H}|j,s^*\rangle,$$

$$E_{p_x,j} = \langle j,p_x|\mathbf{H}|j,p_x\rangle, \quad V_{c,s}^{a,s} = \langle a,s|\mathbf{H}|c,s\rangle,$$

$$V_{c,p_x}^{a,s} = \langle a,s|\mathbf{H}|c,p_x\rangle, \quad V_{a,p_x}^{c,s} = \langle c,s|\mathbf{H}|a,p_x\rangle,$$

$$V_{c,p_x}^{a,s^*} = \langle a,s^*|\mathbf{H}|c,p_x\rangle, \quad V_{a,p_x}^{c,s^*} = \langle c,s^*|\mathbf{H}|a,p_x\rangle,$$

$$V_{c,p_x}^{a,p_x} = \langle a,p_x|\mathbf{H}|c,p_x\rangle, \quad V_{a,p_y}^{c,p_x} = \langle c,p_x|\mathbf{H}|a,p_y\rangle, \tag{4}$$

where $j=a$ or c with a standing for an anion site and c for a cation site. The addition of a spin-orbit coupling term,

$$\mathbf{H}_{SO} = \frac{\hbar}{4m^2c^2}[\nabla V(\mathbf{r})\times\mathbf{p}]\cdot\boldsymbol{\sigma}, \tag{5}$$

to the Hamiltonian requires the use of the basis set of ten orbitals per atom in the sp^3s^* model. Considering only intratomic contributions from p orbitals, the nonzero elements of the spin-orbit coupling term are

$$\langle j,p_x,\uparrow|\mathbf{H}_{SO}|j,p_y,\uparrow\rangle = -i\lambda_j,$$

$$\langle j,p_x,\downarrow|\mathbf{H}_{SO}|j,p_y,\downarrow\rangle = i\lambda_j,$$

$$\langle j,p_x,\downarrow|\mathbf{H}_{SO}|j,p_z,\uparrow\rangle = -\lambda_j,$$

$$\langle j,p_x,\uparrow|\mathbf{H}_{SO}|j,p_z,\downarrow\rangle = \lambda_j,$$

$$\langle j,p_y,\uparrow|\mathbf{H}_{SO}|j,p_z,\downarrow\rangle = -i\lambda_j,$$

$$\langle j,p_y,\downarrow|\mathbf{H}_{SO}|j,p_z,\uparrow\rangle = -i\lambda_j, \tag{6}$$

and their complex conjugates, where $\lambda_j=\lambda_a$ or λ_c.

The number of atoms in the unit cell increases quadratically with the lateral size of the nanowire, ranging from a

few hundred up to about 20 thousand atoms for nanowires with the lateral size of 4 to 30 nm. The latter corresponds to a Hamiltonian matrix in the order of $\sim 10^5 \times 10^5$ in size. Evidently, it is not always possible to solve the eigenvalue problem for the Hamiltonian using a direct diagonalization method. However, since each row only contains a maximum number of 23 nonzero elements [cf. Eqs. (4) and (6)], the Hamiltonian becomes highly sparse as the number of atoms in the unit cell increases. Thus, in this work, the Lanczos recursion algorithm is used to reduce the Hamiltonian matrix to a tridiagonal form.[37] From a starting vector $|0\rangle$, the Lanczos recursion method generates a new basis set of vectors, $\{|0\rangle, |1\rangle, \ldots, |M\rangle\}$, in which the Hamiltonian matrix is in a tridiagonal form $\mathbf{H}_T$ with the dimension $M \leqslant N_H$, where N_H is the size of the original tight-binding Hamiltonian matrix $\mathbf{H}$. The recursion relations are,

$$|1\rangle = \frac{(\mathbf{H} - a_0)|0\rangle}{b_1}, \tag{7}$$

$$|j+1\rangle = \frac{[(\mathbf{H} - a_j)|j\rangle - b_j|j-1\rangle}{b_{j+1}}, \quad 1 \leqslant j \leqslant M. \tag{8}$$

The diagonal and subdiagonal elements of $\mathbf{H}_T$ are a_j and b_j, respectively, and are obtained by imposing the orthonormal condition on the vectors $\{|0\rangle, |1\rangle, \ldots, |M\rangle\}$. Mathematically, it can be shown that the vectors $\{|0\rangle, |1\rangle, \ldots, |M\rangle\}$ are exactly orthogonal to each other. However, in numerical calculations, the orthogonality of these vectors quickly deteriorates as the number of recursion steps increases. The problem can be prevented by providing a reorthogonalization scheme. However, this is a computationally costly procedure and is only practical for relatively small structures containing, e.g., a few thousand atoms. For large structures as considered in this work the Lanczos algorithm is used without any reorthogonalization and the wave function is calculated using an inverse iteration method.[40]

As the highest and lowest eigenvalues in the eigenvalue spectra of the matrix are the first to converge in the Lanczos algorithm, the $(\mathbf{H}-\lambda\mathbf{I})^2$ operator is used to fold the energy spectra around an energy λ in the band gap.[38] In this work, λ is chosen to be close to a band edge, taking advantage of the band gap to identify the eigenvalues as either valence or conduction band states.

From Eqs. (7) and (8) it can be shown that only vectors with a finite projection on the starting vector, $|0\rangle$, are generated in the Lanczos recursion procedure. As a consequence, when solving for the eigenvalues for the tridiagonal Lanczos Hamiltonian, only the eigenvalues of $\mathbf{H}$ with eigenvectors that have a nonzero projection on the starting vector are found. This fact is used to divide the task of calculations for the eigenvalues of the Hamiltonian $\mathbf{H}$ according to the irreducible representations of the symmetry group, thus reducing the number of recursions needed to reach convergence. Another advantage of doing calculations within each irreducible representation is that numerical troubles with band crossings and band degeneracy can be avoided. The procedure starts by setting up a symmetrized starting vector using the following projection operator:[39]

$$\mathcal{P}_{kk}^{(j)} = \frac{l_j}{h} \sum_R \Gamma^{(j)}(R)_{kk}^* P_R. \tag{9}$$

Applying this operator to a function $\phi_n(\mathbf{r})$ will project out the part of the function which belongs to the kth row of the jth representation,

$$\phi_{n,k}^{(j)}(\mathbf{r}) = \mathcal{P}_{kk}^{(j)} \phi_n(\mathbf{r}). \tag{10}$$

A starting vector can then be written as

$$\phi_k^{(j)}(\mathbf{r}) = C \sum_n A_n \phi_{n,k}^{(j)}(\mathbf{r}), \tag{11}$$

where C is the normalization constant. The choice of A_n can be used to optimize the shape of the starting vector for achieving fast convergence of a special eigenvalue. In this work we have chosen starting vectors with nonzero elements on the atomic orbitals at positions close to the center of the nanowire.

Due to the loss of orthogonality in the Lanczos basis set, the band-state wave functions of the nanowire are not directly available from the solutions to the Lanczos Hamiltonian. Instead they are calculated using an inverse iteration scheme.[40] In this scheme the wave function corresponding to the eigenvalue E_n is calculated by iteratively solving

$$(\mathbf{H} - \lambda_n \mathbf{I})|b_{k+1}\rangle = |b_k\rangle. \tag{12}$$

Here the starting vector,

$$|b_0\rangle = \sum_j \beta_j |j, \mathbf{k}\rangle, \tag{13}$$

can be any vector as long as it has a finite projection on the wave function $|n, \mathbf{k}\rangle$. The part of the function $|b_k\rangle$ that projects onto $|n, \mathbf{k}\rangle$ will be increased by a factor

$$\alpha_n = \frac{1}{E_n - \lambda_n}, \tag{14}$$

after each iteration. Here, E_n is the true eigenvalue and $\lambda_n = E_n + \Delta E$, where ΔE is an introduced error. In the calculations ΔE is chosen to be small enough to reach the desired accuracy, but large enough to keep Eq. (12) from becoming singular. The method usually converges within three to four iterations. The solution to the large linear system defined by Eq. (12) is found by using a biconjugate gradient method.[40] In the case of degenerate eigenvalues, the method will generate a linear combination of the corresponding wave functions. In order to separate the wave functions of the degenerate states, the projection operator, Eq. (9), is used to project out the wave functions with different symmetries.

B. The nanowire model

In this work, freestanding nanowires oriented along the [100] crystallographic direction have been studied. The nanowires have a square or rectangular cross section and {011} facets, see Fig. 1. The size of the cross section is defined by the distances, d_1 and d_2, between parallel surfaces as shown in Fig. 1. The nanowires are periodic along the [100] direction with a period of $l=a$, where a is the lattice constant

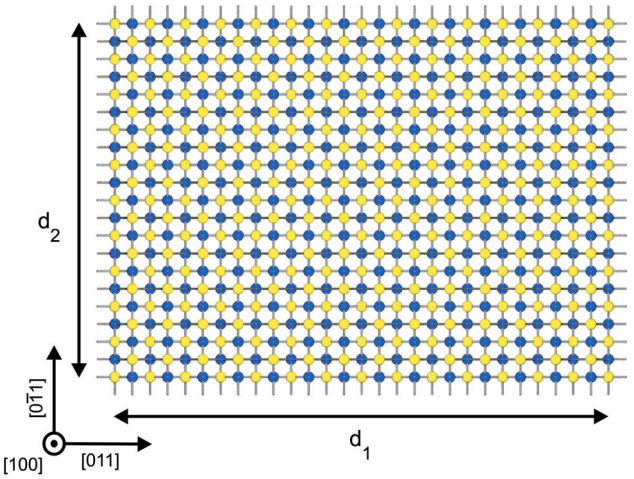

FIG. 1. (Color online) Example of a unit cell for a [100]-oriented nanowire with a lateral size of $d_1 \times d_2$. The surface is passivated by hydrogenlike pseudoatoms (not shown in the figure).

of the corresponding bulk materials. This corresponds to a Brillouin zone with a length of $2\pi/a$. A nanowire with a square cross section has the symmetry of the D_{2d} point group with the principal axis along the [100] direction. However, at $k \neq 0$ the symmetry of the band structure Hamiltonian is described by the C_{2v} point group. For a nanowire with a rectangular cross section, the lattice structure as well as the band structure Hamiltonian have the symmetry of the point group C_{2v}, with the principal axis again along the [100] direction. The starting vector in the Lanczos algorithm was symmetrized according to the C_{2v} point group for the band-structure calculations of both the square and rectangular nanowires, while it was symmetrized according to the D_{2d} point group for the calculation of the wave functions of the square nanowire at the Γ point ($k=0$).

The surface dangling bonds of the nanowires have been passivated using hydrogenlike pseudoatoms. The onsite energy of the hydrogenlike pseudoatoms is determined from the difference between the s orbital energy of the neutral hydrogen atom and the s orbital energies of the nanowire host atoms (in the neutral state) using a procedure described by Vogl *et al.*[36] The interaction parameters between the hydrogenlike pseudoatoms and the nanowire host surface atoms are determined using the Wolfsberg-Helmholz formula[41] in a procedure described by Xu and Lindefelt[42–45] in such a way that the surface states are pushed to locate in energies far remote from the fundamental band gap. It should be noted that in a free-standing nanowire, surface lattice relaxation, and reconstruction can occur. However, the surface relaxation and reconstruction mainly affect the surface electron states which, in a surface passivated nanowire, have energies far remote from the fundamental band gap. Thus the effects of surface relaxation and reconstruction have been neglected in this work. The tight-binding parameters used in this work to describe the passivated surfaces are given in Table II.

TABLE II. Tight-binding parameters used in this work to describe the hydrogenlike pseudoatom-passivated surfaces. The parameters are given in eV and are derived by taking the distance between the hydrogenlike pseudoatoms and the nanowire host atoms as $0.4l_b$, where l_b is the bond length of the bulk materials.

Material	$E_{H,s}$	$V_{H,s}^{a,s}$	$V_{H,s}^{c,s}$	$V_{a,p_x}^{H,s}$	$V_{c,p_x}^{H,s}$
InAs	−5.525	−6.676	−7.587	2.405	6.002
InP	−4.470	−7.721	−8.823	3.394	6.447

III. RESULTS AND DISCUSSION

As symmetry plays an important role in the understanding of electrical and optical measurements we will start by discussing the symmetry of the nanowire systems. For the bulk materials the double-valued T_d point group allows for two double degenerate representations and one fourfold degenerate representation; the latter is manifested by the degeneracy between the valence light- and heavy-hole bands at the Γ point. However, in the case of a nanowire with a square (rectangular) cross section the crystallographic structure is symmetric under the operations of the D_{2d} (C_{2v}) point group. Neither of these groups allows for a fourfold degenerate double-valued irreducible representation. Consequently, the light- and heavy-hole degeneracy in the bulk materials is lifted in the nanowires. For the square nanowire it should be noted that the band structure Hamiltonian at the Γ point ($k=0$) is invariant under the symmetry operations of the D_{2d} group, which has two double-degenerate double-valued irreducible representations, Γ_6 and Γ_7. At $k \neq 0$ the Hamiltonian has the same symmetry as for the rectangular nanowire, namely it is invariant under the symmetry operations of the C_{2v} group. The C_{2v} group only allows for one double-degenerate double-valued irreducible representation, Γ_5.[46] This is in contrast to $\mathbf{k}\cdot\mathbf{p}$ theory in which the bands of a square nanowire are characterized according to the irreducible representations of the C_{4v} group.[18] As a result not all anticrossings seen in our calculations, can be observed in a calculation based on $\mathbf{k}\cdot\mathbf{p}$ theory. This difference is due to the fact that the lack of crystalline structure in the $\mathbf{k}\cdot\mathbf{p}$ model results in an unphysical, higher symmetry for a square nanowire.

A. Band structure

Figures 2 and 3 show the band structure of an InAs nanowire with the size 13×13 nm^2 and an InP nanowire with the size 12.5×12.5 nm^2, respectively. The symmetry of the band states at the Γ point are marked as Γ_6 or Γ_7 in each figure according to the double-valued irreducible representations of the D_{2d} point group.

For both materials the conduction bands show good parabolic dispersions around the Γ point, although the effective mass of the bands are enhanced as a result of the nonparabolicity in the corresponding bulk conduction bands.[33] Due to spin-orbit coupling the second and third conduction bands are not degenerate (except for the spin degeneracy), different from the prediction based on a one-band effective-mass model. The energy separation between the two bands is, however, small but distinguishable for the InAs nanowire. While for the InP nanowire it is almost indistinguishable. A very small energy separation of the second and third conduc-

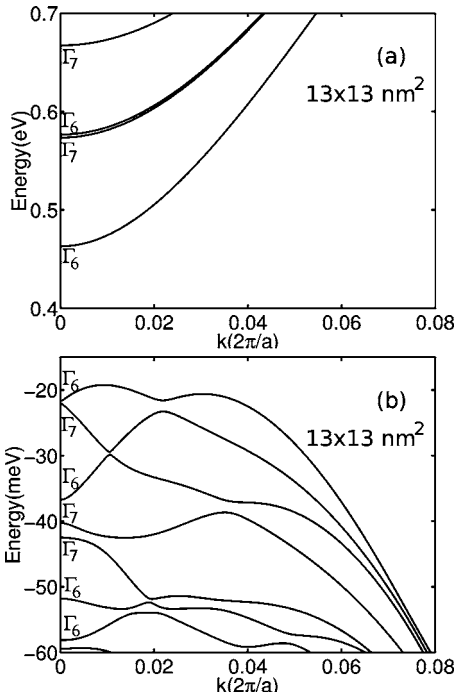

FIG. 2. Band structure of the [100]-oriented InAs nanowire with a square cross section of the size 13×13 nm^2. The symmetries of the band state at the Γ point are marked according to the double-valued irreducible representations, Γ_6 and Γ_7, of the D_{2d} point group.

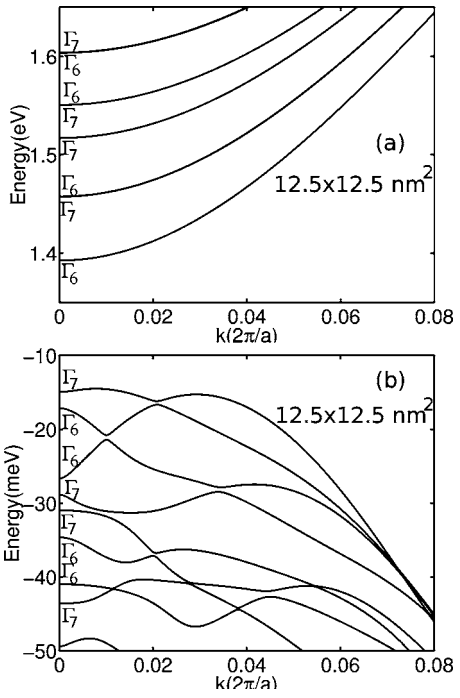

FIG. 3. Band structure of the [100]-oriented InP nanowire with a square cross section of the size 12.5×12.5 nm^2. The symmetries of the band state at the Γ point are marked according to the double-valued irreducible representations, Γ_6 and Γ_7, of the D_{2d} point group.

tion bands was also found for the GaAs square nanowires.[33]

The valence bands of the square nanowires show rich and complex structures such as strong nonparabolicity, anticrossings, and a double-maximum structure in the highest valence band. By comparing the valence band structures of the InAs and InP nanowires we find that for sizes larger than $d\approx12.5$ nm, the symmetry ordering of the two highest valence band states of the two material types of square nanowires at the Γ point is different. The two states in the InP nanowires have the same symmetry ordering as in the GaAs nanowires, while the two states in the InAs nanowires have the reverse ordering of symmetries. For the InP and InAs nanowires with sizes smaller than $d\approx12.5$ nm the two highest valence band states have the same symmetry ordering as in the GaAs nanowires (cf. Ref. 33). In general, the four highest valence bands of the InAs, GaAs, and InP nanowires are found to have similar band structure characteristics, except for the difference in the symmetry ordering of the states at the Γ point. Also, by comparing the valence bands for different nanowire sizes we see that the general band-structure characteristics are insensitive to the change of the nanowire size, although the band energies depend sensitively on the nanowire size and the anticrossings in the valence bands become more pronounced for small nanowire sizes.

It is interesting to study how the band structure develops when the cross section of the nanowire becomes rectangular. Here we do not discuss the development of the conduction bands, since they show rather simple dispersion relations similar to the results for the rectangular GaAs nanowires as shown in Ref. 33. Free-standing nanowires with large cross-section aspect ratios, $A=d_1/d_2$, are often referred to as nanobelts. In Fig. 4 the valence band structures for InAs nanowires with sizes of 26×13 nm^2 ($A=2$), 51×13 nm^2 ($A=4$), and 77×13 nm^2 ($A=6$) are shown. At $A=2$ some resemblance to the valence band structure of the square wires can still be seen, while the anticrossings between bands have become more pronounced. As the aspect ratio is further increased, e.g., at $A=4$, the highest valence band starts to show good parabolicity around the Γ point, while lower lying bands remain nonparabolic. At $A=6$, the second highest valence band also becomes parabolic around the Γ point. The parabolicity of the topmost bands can be understood as a result of decoupling of these topmost $(01\bar{1})$-oriented quantum-well-like bands from all the other bands. Also, the second maximum of the highest valence band, previously seen in a square nanowire, becomes less pronounced as the aspect ratio of the nanowire is increased.

The valence band structure of the InP nanowires shows the same characteristics as the InAs nanowire with some minor differences. Figure 5 shows the valence bands for InP nanowires with sizes of 25×12.5 nm^2 ($A=2$), 50×12.5 nm^2 ($A=4$), and 75×12.5 nm^2 ($A=6$). As for the InAs nanowire, the topmost valence band of the InP nanowire at $A=4$ and 6 is of a parabolic type around the Γ point. Compared to the InAs nanowire with the same aspect ratio the InP nanowire tends to have more parabolic valence bands. The second maximum of the highest valence band, found for the square nanowires, is more quickly suppressed in the rectangular InP nanowire; this maximum remains to be clearly identified in Fig. 5 only for the case of the aspect ratio $A=2$.

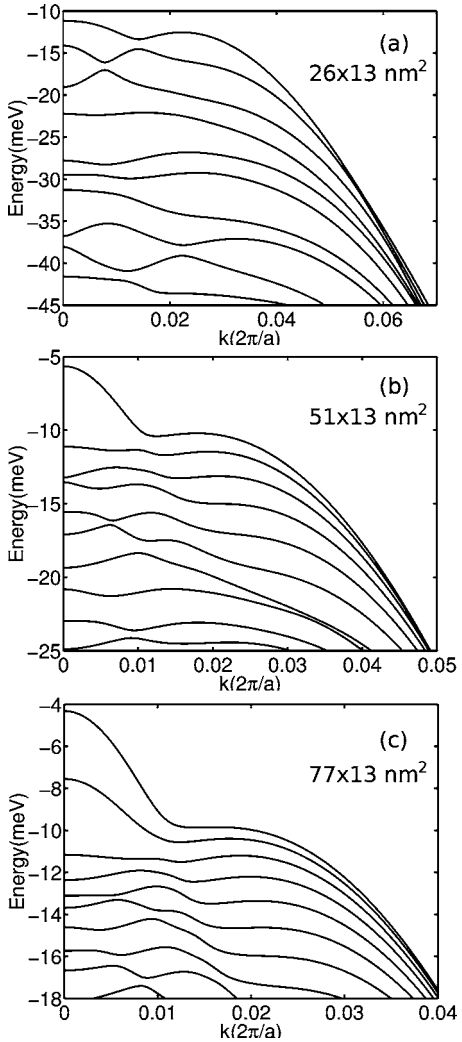

FIG. 4. Valence band structure of the [100]-oriented InAs nanowires with a rectangular cross section of the size (a) 26×13 nm^2, (b) 51×13 nm^2, and (c) 77×13 nm^2.

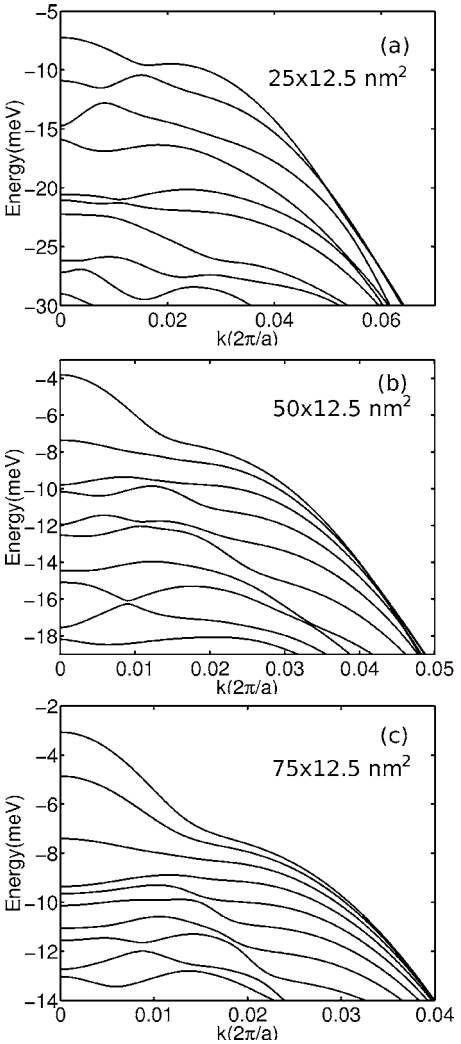

FIG. 5. Valence band structure of the [100]-oriented InP nanowires with a rectangular cross section of the size (a) 25×12.5 nm^2, (b) 50×12.5 nm^2, and (c) 75×12.5 nm^2.

Comparing the band structure of the InAs, InP, and GaAs nanowires shows that disregarding the difference in energy scale, all three material types of nanowires show simple, parabolic conduction-band dispersion relations. The valence band structure of the three material types of nanowires shows strong dependence on the aspect ratio of the cross section. For the nanowires with a square cross section, the valence bands show rich and complex structures. In particular, the highest valence band of a square nanowire shows a double-maximum structure and has its energy maximum at $k\neq0$, giving an indirect nanowire band gap. When the cross section of the nanowires changes from square to rectangular type, the top valence bands tend to develop into parabolic bands. However, the InAs nanowire keeps the double-maximum structure in its highest valence band to a larger aspect ratio of the cross section than the other two material types of nanowires. For the nanowires with the same cross-section aspect ratio and material type, the valence band structures at different sizes are found to have similar characteristic structures, although the band energies sensitively depend on the nanowire lateral size.

B. Wave functions

For a better understanding of the nature of the energy band structure of the nanowires it is valuable to study the wave functions of the band states at the Γ point. As the nature of the conduction band states is fairly well understood, we will focus on the wave functions of the valence band states and discuss how they evolve as the cross-section aspect ratio is changed. The wave function is represented by the probability distribution on a (100)-plane of anion (As or P) atoms, calculated at each atomic site by summing up the squared amplitudes of all the atomic orbital components on that site. In the figures, only one of the spin-degenerate wave functions is presented since the other one has an identical spatial part. The four (100)-layers of atoms in a unit cell have rather similar probability distributions, though a difference in amplitude can be identified between the probability distributions on the cation and anion layers.

Figures 6(a)–6(d) and Figs. 6(e)–6(h) show the probability distribution of the four highest valence band states at the Γ point for a square InAs nanowire with the size 13

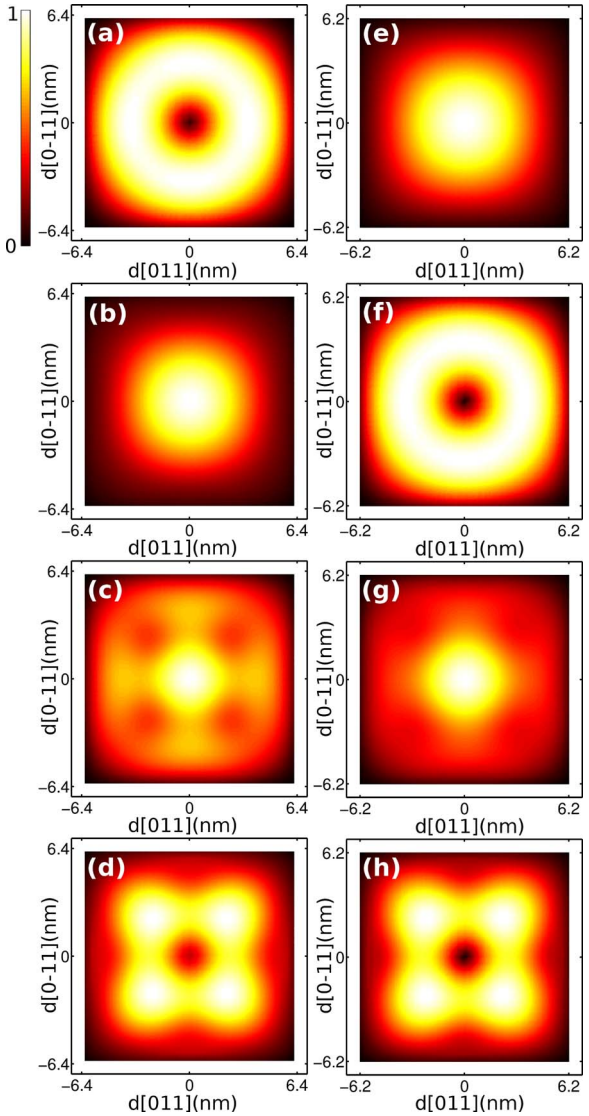

FIG. 6. (Color online) Probability distributions of the wave functions of the four highest valence band states at the Γ point for (a)–(d) the InAs square nanowire with the size 13×13 nm^2 and (e)–(h) the InP square nanowire with the size 12.5×12.5 nm^2. The corresponding band structures are shown in Fig. 2(b) and Fig. 3(b). Here, the wave function is represented by the probability distribution on a (100)-plane of anion (As or P) atoms, calculated at each atomic site by summing up the squared amplitudes of all the atomic orbital components on that site. Within each graph, the probability distribution for one of the two spin-degenerate wave functions, scaled against its maximum value, is plotted.

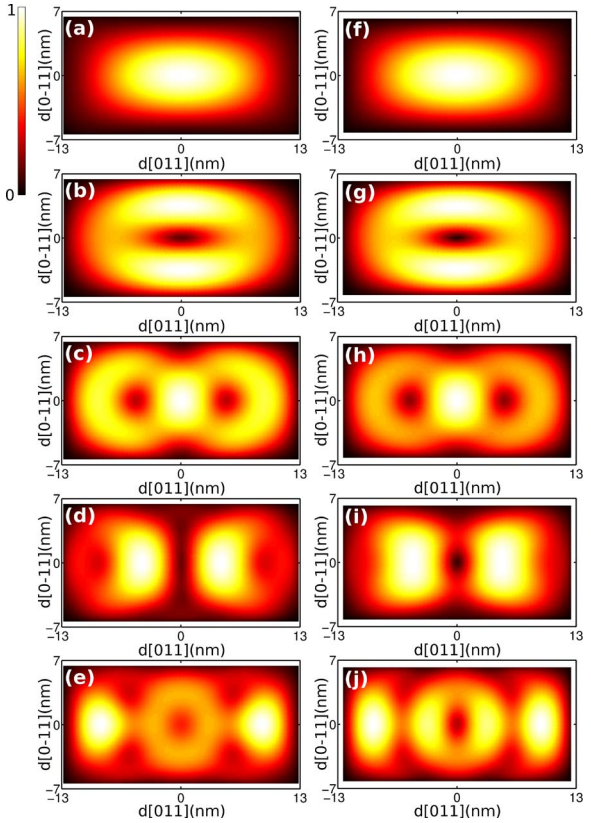

FIG. 7. (Color online) Probability distributions of the wave functions of the five highest valence band states at the Γ point for (a)–(e) the rectangular InAs nanowire with the size 26×13 nm^2 and (f)–(j) the rectangular InP square nanowire with the size 25×12.5 nm^2. The corresponding band structures are shown in Fig. 4(a) and Fig. 5(a). Here, the wave function is represented by the probability distribution on a (100)-plane of anion (As or P) atoms, calculated at each atomic site by summing up the squared amplitudes of all the atomic orbital components on that site. Within each graph, the probability distribution for one of the two spin-degenerate wave functions, scaled against its maximum value, is plotted.

$\times13$ nm^2 and for a square InP nanowire with the size 12.5 $\times12.5$ nm^2, respectively. The highest valence band state of the InP nanowire is *s* like, while the highest valence band state of the InAs nanowire is of donut shape with a central node. For the second highest valence band state the situation is reversed, i.e., the state in the InAs nanowire is *s* like, while the state in the InP nanowire is of donut shape. These results agree with the attributed symmetries of the two highest valence band states of the two nanowires at the Γ point (see Figs. 2 and 3). The third highest valence band states of the InP and InAs nanowires have large contributions from atomic orbitals close to the surface and a slightly cross-shaped probability distribution. These wave function characteristics are particularly clear in the plot for the third highest valence band states of the InAs nanowire [Fig. 6(c)]. The fourth valence band states of the two square nanowires are localized in four lobes oriented towards the four corners of the cross section. Note that the valence band states of the square GaAs nanowire have similar wave function characteristics as in the InP nanowire (cf. Ref. 33).

For the rectangular nanowires we show the results of the calculations for two aspect ratios, namely $A=2$ and $A=6$. First we show in Fig. 7 the probability distribution of the wave functions of the five highest valence band states at the Γ point for an InAs nanowire with the size 26×13 nm^2 and for an InP nanowire with the size 25×12.5 nm^2 (both have an aspect ratio of $A=2$). It is seen in the figure that the highest valence band state now is *s* like in both the InAs and the InP nanowire. The second valence band state retains some of its donut shape although now with an increased

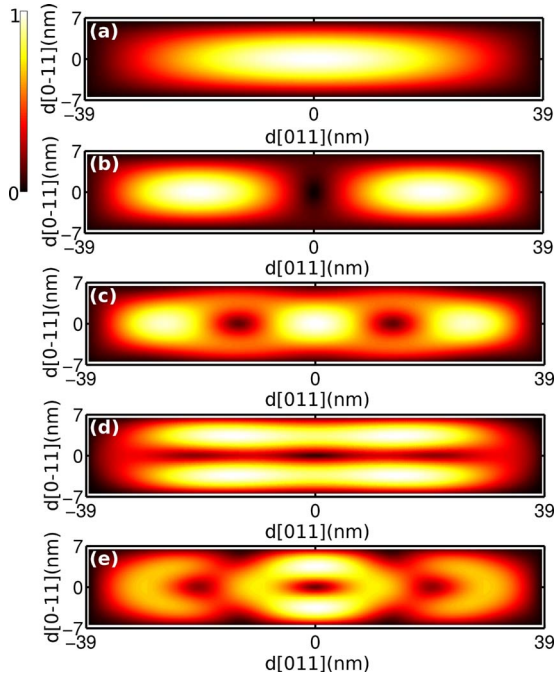

FIG. 8. (Color online) The same as in Fig. 7 but for the five highest valence band states, at the Γ point, of an rectangular InAs nanowire with the size 77×13 nm^2. The corresponding band structure is shown in Fig. 4(c).

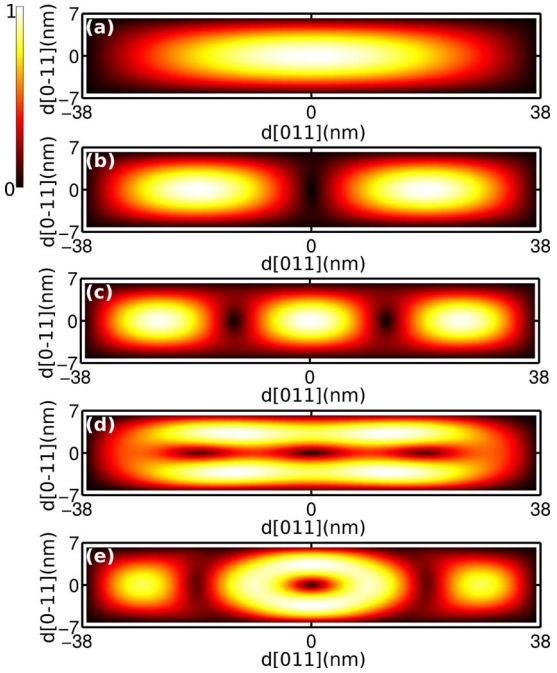

FIG. 9. (Color online) The same as in Fig. 7 but for the five highest valence band states, at the Γ point, of an rectangular InP nanowire with the size 75×12.5 nm^2. The corresponding band structure is shown in Fig. 5(c).

concentration in the regions close to the elongated facets. Also the wave function of the third valence band state has retained some likeness to the third valence band state of the square nanowire with a strong contribution from atoms close to the center of the nanowire. Comparing the wave functions between the InAs and InP nanowires we see that the wave functions of all the five states have similar probability distributions in agreement with the fact that the two rectangular nanowires have similar valence band structures.

We now show the wave function calculations for the rectangular nanowires with the aspect ratio $A=6$ for which the two topmost valence bands were found to be of parabolic type around the Γ point. Figure 8 shows the probability distribution of the wave functions of the five highest valence band states at the Γ point for the InAs nanowire with the size 77×13 nm^2. Since the two topmost valence bands of the nanowire are of parabolic type, we expect the two corresponding band states at the Γ point to show the characteristics of the wave functions that can be derived from a one-band effective-mass model. Indeed, both the first and the second highest valence band state have probability distributions similar to what one would expect from a one-band effective-mass model. The wave function of the highest valence band state has an *s*-like probability distribution and the second valence band state has a probability distribution that is concentrated in two areas with a node line in the middle. The probability distribution of the third band state is concentrated in three areas, similar to the prediction by a single-band model. However, here the areas are connected by arms surrounding a node. The probability distributions of the fourth and fifth highest valence band states show no similarities to what one would expect based on a simple one-band model, in agreement with the fact that these states belong to nonparabolic bands. In general we find that as the aspect ratio is decreased and the parabolic bands become nonparabolic their wave functions lose similarity to the predictions of a one-band effective-mass model.

The wave function characteristics as seen in the rectangular InAs nanowire can also be seen in the InP nanowires. Figure 9 shows the five highest valence band states at the Γ point for the InP nanowire with the size 75×12.5 nm^2 ($A=6$). Here, the three highest valence band states have probability distributions similar to the prediction of a single-band model, in agreement with the fact that the three corresponding valence bands are of the parabolic type in this rectangular InP nanowire. States four and five of the InP nanowire share no features of the single-band model prediction as the corresponding bands are nonparabolic. The probability distribution of the fourth valence band state is similar to that of the fourth InAs valence band state, while the fifth valence band state of the InP nanowire has a slightly different probability distribution from that in the InAs nanowire.

IV. CONCLUSIONS

The band structure and wave functions of [100]-oriented freestanding InAs and InP nanowires have been studied using an atomistic tight-binding approach. The effects of cross-section aspect ratio on the band structure and wave functions have been studied. It has been shown that at the same cross-section aspect ratio, the characteristics of the band structure of the nanowires are insensitive to the variation of the lateral size, although the band energies show a strong dependence

on the lateral size. For the nanowires with a square cross section the valence band structure is found to be strongly nonparabolic. As the cross-section aspect ratio is increased, the nonparabolicity of the valence bands is reduced and the highest valence bands tend to show good parabolicity around the Γ point. It has also been shown that both the square and the rectangular nanowires have simple, parabolic type conduction bands. The band structures of InAs, InP, and GaAs nanowires are compared. It is found that they have much in common, despite of the significant differences in the bulk band-gap energy and electron and light-hole masses. The wave functions of the valence band states at the Γ point have been calculated for the InAs and InP nanowires. It is found that for the square nanowires the valence band states show complex structures. For the rectangular nanowires with sufficiently large aspect ratios the wave functions of the highest valence band states show the features expected from a one-band effective-mass model, in agreement with the fact that these valence bands become good parabolic bands in these large aspect-ratio rectangular nanowires.

ACKNOWLEDGMENTS

This work was supported by the Swedish Research Council (V.R.) and the Swedish Foundation for Strategic Research (S.S.F.) through the Nanometer Structure Consortium at Lund University and by the European Project No. MRTN-CT-2003-503677 "CLERMONT II."

*Electronic address: Paul.Martin.Persson@uniroma2.it
†Electronic address: Hongqi.Xu@ftf.1th.se

[1] R. S. Wagner, in *Whisker Technology*, edited by A. P. Levitt (Wiley, New York, 1970), pp. 47–119.
[2] Y. Xia, P. Yang, Y. Sun, Y. Wu, B. Mayers, B. Gates, Y. Yin, F. Kim, and H. Yan, Adv. Mater. **15**, 353 (2003).
[3] A. D. Kimberly, K. Deppert, L. S. Karlsson, L. R. Wallenberg, L. Samuelson, and W. Seifert, Adv. Funct. Mater. **15**, 1603 (2005).
[4] K. Hiruma, M. Yazawa, T. Katsuyama, K. Ogawa, K. Haraguchi, M. Koguchi, and H. Kakibayashi, J. Appl. Phys. **77**, 447 (1995).
[5] U. Krishnamachari, M. Borgström, B. Ohlsson, N. Panev, L. Samuelson, and W. Seifert, Appl. Phys. Lett. **85**, 2077 (2004).
[6] M. S. Gudiksen, J. Wang, and C. M. Lieber, J. Phys. Chem. B **105**, 4062 (2001).
[7] K. Haraguchi, T. Katsuyama, and K. Hiruma, J. Appl. Phys. **75**, 4220 (1994).
[8] B. J. Ohlsson, M. T. Björk, A. I. Persson, C. Thelander, L. R. Wallenberg, M. H. Magnusson, K. Deppert, and L. Samuelson, Physica E (Amsterdam) **13**, 1126 (2002).
[9] X. Duan, Y. Huang, Y. Cui, J. Wang, and C. M. Lieber, Nature (London) **409**, 66 (2001).
[10] M. T. Björk, B. J. Ohlsson, C. Thelander, A. I. Persson, K. Deppert, L. R. Wallenberg, and L. Samuelson, Appl. Phys. Lett. **81**, 4458 (2002).
[11] M. T. Björk, B. J. Ohlsson, T. Sass, A. I. Persson, C. Thelander, M. H. Magnusson, K. Deppert, L. R. Wallenberg, and L. Samuelson, Appl. Phys. Lett. **80**, 1058 (2002).
[12] M. S. Gudiksen, L. J. Lauhon, J. Wang, D. C. Smith, and C. M. Lieber, Nature (London) **415**, 617 (2002).
[13] J. C. Johnson, H.-J. Choi, K. P. Knutsen, R. D. Schaller, P. Yang, and R. J. Saykally, Nat. Mater. **1**, 106 (2002).
[14] J. C. Johnson, H. Yan, P. Yang, and R. J. Saykally, J. Phys. Chem. B **107**, 8816 (2003).
[15] D. Li, Y. Wu, L. Shi, P. Yang, and A. Majumdar, Appl. Phys. Lett. **83**, 2394 (2003).
[16] D. D. D. Ma, C. S. Lee, F. C. K. Au, S. Y. Tong, and S. T. Lee, Science **299**, 1874 (2003).
[17] X. Duan, Y. Huang, R. Agarwal, and C. M. Lieber, Nature (London) **421**, 241 (2003).
[18] D. S. Citrin and Y.-C. Chang, Phys. Rev. B **40**, 5507 (1989).
[19] P. C. Sercel and K. J. Vahala, Phys. Rev. B **44**, 5681 (1991).
[20] A. A. Yamaguchi and A. Usui, Mater. Sci. Eng., B **35**, 288 (1995).
[21] Y. Arakawa, T. Yamauchi, and J. N. Schulman, Phys. Rev. B **43**, 4732 (1991).
[22] F. Vouilloz, D. Y. Oberli, M.-A. Dupertuis, A. Gustafsson, F. Reinhardt, and E. Kapon, Phys. Rev. B **57**, 12378 (1998).
[23] T. Someya, H. Akiyama, and H. Sakaki, Phys. Rev. Lett. **74**, 3664 (1995).
[24] P. Ils, C. Gréus, A. Forchel, V. D. Kulakovskii, N. A. Gippius, and S. G. Tikhodeev, Phys. Rev. B **51**, 4272 (1995).
[25] A. Di Carlo, S. Pescetelli, A. Kavokin, M. Vladimirova, and P. Lugli, Phys. Rev. B **57**, 9770 (1998).
[26] L. C. Lew Yan Voon, B. Lassen, R. Melnik, and M. Willatzen, J. Appl. Phys. **96**, 4660 (2004).
[27] M. P. Persson and H. Q. Xu, Appl. Phys. Lett. **81**, 1309 (2002).
[28] M. P. Persson and H. Q. Xu, Phys. Rev. B **70**, 161310(R) (2004).
[29] J. Li and L.-W. Wang, Nano Lett. **4**, 29 (2004).
[30] Y. Zheng, C. Rivas, R. Lake, K. Alam, T. B. Boykin, and G. Klimeck, IEEE Trans. Electron Devices **52**, 1097 (2005).
[31] Y. M. Niquet, C. Delerue, G. Allan, and M. Lannoo, Phys. Rev. B **62**, 5109 (2000).
[32] A. Franceschetti and A. Zunger, Appl. Phys. Lett. **68**, 3455 (1996).
[33] M. P. Persson and H. Q. Xu, Nano Lett. **4**, 2409 (2004).
[34] M. P. Persson, and H. Q. Xu, Phys. Rev. B **73**, 035328 (2006).
[35] G. Klimeck, R. C. Bowen, T. B. Boykin, and T. A. Cwik, Superlattices Microstruct. **27**, 519 (2000).
[36] P. Vogl, H. P. Hjalmarson, and J. D. Dow, J. Phys. Chem. Solids **44**, 365 (1983).
[37] G. H. Golub and C. F. Van Loan, *Matrix Computations*, 3rd ed. (The Johns Hopkins University Press, Baltimore, 1996).
[38] L.-W. Wang and A. Zunger, J. Chem. Phys. **100**, 2394 (1994).
[39] M. Tinkham, *Group Theory and Quantum Mechanics* (McGraw-Hill, New York, 1964).
[40] W. H. Press, S. A. Teukolsky, W. T. Vetterling, and B. P. Flannery, *Numerical Recipes in C: The Art of Scientific Computing*, 2nd ed. (Cambridge University Press, Cambridge, 1992).
[41] M. Wolfsberg and L. Helmholz, J. Chem. Phys. **20**, 837 (1952).
[42] H. Xu and U. Lindefelt, Phys. Rev. B **41**, 5979 (1990); H. Xu, *ibid.* **42**, 11295 (1990).
[43] H. Q. Xu, J. Appl. Phys. **68**, 4077 (1990).
[44] H. Xu, Phys. Rev. B **46**, 1403 (1992).
[45] N. A. Hill and K. B. Whaley, Phys. Rev. Lett. **75**, 1130 (1995).
[46] P. Y. Yu and M. Cardona, *Fundamentals of Semiconductors*, 3rd ed. (Springer, Berlin, 2001).